電波及正常星系之核心灰塵特徵

吳思瑩、孫維新
國立中央大學天文研究所

摘要

我們對一些電波星系做統計上的研究，爲了瞭解我們可以多常偵測到核心附近的光學噴流、環心的灰塵盤、灰塵帶，或灰塵纖維狀結構。且想進一步找出灰塵的存在是否與它們的無線電波性質之間有關聯。我們總共用了 46 個距離我們較近的電波星系之哈伯望遠鏡觀測資料，它們皆是含有無線電波噴流，但沒有發表過伴隨著有光學波段噴流的星系。星系模型扣除原影像後，並沒有發現在星系中心附近有任何明顯的光學特徵，然而，在這些星系中，有 22 個（大約 48％）出現了深色類似灰塵盤、灰塵帶、甚至纖維狀結構。有些星系我們已證實前人已發表過，但是仍有一些星系是別人尚未發現過的，像是 PKS2152-69 這個星系。未來進一步的研究將會探討它們之間的物理及核心灰塵和周遭環境的關係。

Nuclear Dust Features in Radio and Normal Galaxies

Wu Szu-Ying, Sun Wei-Shin
Institute of Astronomy, National Central University

Abstract

We have carried out a statistical study of a large sample of radio galaxies in order to understand how frequently we can detect nuclear optical jets, circum-nuclear dust disks, dust lanes, or dust filaments, and to further find out what the relationships are between the existence of dust features and their radio properties. A total of 46 nearby radio galaxies are selected based on their HST/WFPC2 observations, from which radio jets have been detected but without known optical jets. Galaxy model subtractions did not reveal any prominent optical features in or near the nuclei for the sample galaxies. However, among these galaxies, 22 (48%) reveal dark features such as dust disks, lanes, or even filaments. In several sample galaxies, we confirm the main morphological results published by previous authors; while in others, such as in PKS2152-69, we present our new findings of dust features. We also discuss the dust properties along with their radio properties. Further study will be conducted in order to learn more about the physics and the relationships between nuclear dust and the ambient medium.

關鍵字（Key words）：灰塵特徵（dust features）、電波星系（radio galaxies）、正常星系（normal galaxies）、哈伯太空望遠鏡（HST）

1. Research Motivation

Radio galaxies are galaxies identified with sources in radio catalogues. The most famous catalogue was the third survey carried out at Cambridge (the 3C catalogue; Edge et al. 1959), which covered the northern hemisphere at a wavelength of 177 MHz and turned up 471 radio sources brighter than 9Jy; and its successor, the 4C catalogue, contains almost 5,000 sources (Pilkington & Scott 1965; Gower, Scott &Wills 1967). About two-thirds of the bright extra-galactic radio sources appear to be elliptical galaxies. Like Seyfert galaxies, radio galaxies can be divided on the basis of their optical spectra into narrow-line radio galaxies (NLRG) which emit only the narrow emission lines characteristic of Seyfert 2 galaxies, and broad-line radio galaxies (BLRG) which emit the broad lines resembling those from Seyfert 1 galaxies (Kembhavi, A.K. and Narlikar, J.V. 1999).

Detection of stellar disks in radio galaxies is crucial for the understanding of the source of fuel for active galactic nuclei and the stability of the radio axis in large radio sources (Gonzalez -Serrano, J.I. et al. 1989). The dusty ellipticals may also be important for our understanding of the origins of activity in elliptical galaxies. The dust lanes, dust disks, or even filaments could provide information about the dynamics and the true, three-dimensional figures of the galaxies (Ebneter, K. et al. 1985). Besides, the symmetry axis of the nuclear disks may be a useful indicator of the rotation axis of the central black hole (e.g. Capetti & Celotti 1999).

A statistical study of large sample of low luminosity radio galaxies (eg. 1037erg/s) will enable us to know how frequently we can detect optical jets, circum- nuclear dusty disks, dust lanes or filaments and what their relationship to the radio properties. A survey of radio-loud early-type galaxies (Verdoes Kleijn et al. 1999) has shown that the presence of dust is 89%. Sparks et al. (2000) showed that the detection rate of dust and dusty disks in nearby- FR I radio sources are nearly 100%. Capetti, A. et al. (2000) showed that dust is frequently present in B2 sources: after visual inspection of the images they found that 58% of them show dust features, either in the form of bands or disk-like structures, or more irregular patches. This is generally comparable to those reported by previous studies of early-type galaxies, which have shown the following detection rates of dust: Sadler & Gerhard (1985): 40%; V´eron-Cetty & V´eron (1988): 23%; Goudfrooij et al. (1994): 41%; van Dokkum & Franx (1995): 48%; Ferrari et al. (1999): 75%; Tomita et al. (2000): 56%. The large variation in the dust detection rates among different studies may be due to the different methods of counting detections, or the different resolutions and sensitivities of the observations (Tran, H.D. et al. 2001). The Hubble Space Telescope observations have shown the presence of dust in a large fraction of weak (FR I) radio galaxies which takes the form of extended nuclear disks (Jaffe et al. 1993; de Koff et al. 1996; de Juan et al. 1996; Verdoes Kleijn et al. 1999). In a study of eight radio galaxies with dust features, Kotanyi & Ekers (1979) found that in seven cases the dust lane was nearly perpendicular to the axis of the radio source, implying a close connection between the mechanism which collimates the radio-emitting plasma and the rotation axis of the dust lane. de Koff et al. (2000) found that for FR I sources with dust disks of size less than 2.5kpc, the radio jets lie within less than or about 15º of the disk (perpendicular) axis (but with a small number of exceptions such as 3C 31). Why jets and dust lanes are close to perpendicular remains a mystery. Maybe the relaxed, orderly systems have had time to settle down. Their axes and the black holes' spin axes have also had time to co-align.

On the other hand, radio jets have been detected in various types of radio sources but optical jets and X-ray jets are only observed in a handful of objects. It is generally believed that the jets are made detectable, at least in the radio wavelengths, by synchrotron emission from relativistic particles moving in magnetic fields. The physics is still poorly understood, however, for the optical and X-ray jets. The preliminary study reveals that, up until now, among the known radio jets, only 13 objects have optical emission, 24 with X-ray emission, and 13 with both optical and X-ray emission (F.K. Liu and Y.H. Zhang 2002; Jester, S. 2003). With this information, two questions immediately emerge: (1) Why do we see so few optical jets in so many objects possessing radio jets? (2) Are there optical jets hidden and contaminated, and thus unrevealed near the nuclei of the host galaxies?

Martel et al. (1999) noted that disk-like structures are preferentially associated to FR I radio sources. Since FRI sources often have detected radio jets, it is expected that the presence of disklike structures is also related to the presence of jets (de Ruiter, H.R. et al. 2002) Besides, Sparks, W.B. et al. (2000) showed that of the nearest five FR I 3CR radio galaxies showing optical jets, four show evidence for almost circular, presumably face-on, dust disks.

In order to remove the influences of host galaxies and to detect nuclear dust and any other underlying structures, we begin our study using the galaxy images in the HST archive and subtracting elliptical galaxy models. The high resolution of HST images allows us to observe the dust in greater detail and on smaller physical scales than ever before that might help us to find optical jets near the nucleus.

The purpose of this thesis is to present a sample of galaxies with dust features in them, some of which have been reported before while others have not. For those that have been detected before, we confirmed the main morphological results published by previous authors. We also compared the properties of the radio galaxies and the normal galaxies containing dust features. A Hubble constant H_0 = 75kms^{-1}Mpc^{-1} is assumed throughout this thesis.

2. The Galaxy Sample and Data Analysis

2.1 The Galaxy Sample

We selected 46 radio galaxies with radio jets but without known optical jet-like features (according to the list arranged by F.K.Liu (2002); Jester, S. (2003)) in HST data archive. In order to compare the role of radio properties in the presence of dust, we also selected 58 normal galaxies in the HST archive. Table 2.1 and Table 2.2 are basic properties of radio and normal galaxies.

2.2 Data Analysis

Here in this thesis, we made use of the images observed with the WFPC2 on HST. Standard calibration observations are obtained and maintained in the HST archive at the STScI, and can be retrieved by external users. This includes flatfield, dark, and bias reference files needed to operate the Post Observation Data Processing System. For all the radio galaxies, we use the standard task ELLIPSE in STSDAS[1] /IRAF to derive the isophotal morphological parameters. The ELLIPSE task fits elliptical isophotes to galaxy images which best reproduce the observed isophotes of those images (Jedrzejewski 1987). The task reads one 2-dimensional image section and produces as main output one table which contains columns with parameters for each fitted isophote, and one table row for each isophote. The task can be run in interactive mode. Better parameters are found by an iterative procedure.

We then derived a model image for the galaxy from the isophotes fits using the BMODEL task. Then we used the IMARITH task to subtract this galaxy model image from the original data. These attempts have been made to reveal the faint features that might be hidden by the light from the host galaxies.

In order to test the reality and correctness of the task "ELLIPSE", we simulate an elliptical galaxy image with smooth background and a hidden bar near the nucleus. Then we made a galaxy model image from it, and subtract the model image from the original simulated image. As the results showed, the hidden bar is revealed after the subtraction. This demonstration supports our results and suggests that those dark features are not artifacts. "ELLIPSE" really works!

Fig. 2.1: Galaxy original image, Galaxy model image, Residuals

3. Results

Here we present the results of radio and normal galaxies after model subtractions. Out of the 46 radio galaxies, there are 22 that reveal dust features, at a rate about 48%. And there are 14 dusty galaxies from a total of 58 normal galaxies, at a detection rate of about 24%.

Here we describe some dusty radio and normal galaxies in detail. The indications of the radio jets in each galaxy are drawn on the image to the right with white arrows.

3.1 IC 4296

IC 4296 is an FR I radio galaxy. It is a regular elliptical galaxy located at the center of cluster Abell 3565. Its morphology is E0. It reveals large dust patches around the center and some indication of a disk (Colbert, J.W. et al.

[1] STSDAS is the software developed in Space Telescope Science Institute.

Fig. 3.1: IC 4296, IC 4296 model, IC 4296 subtracted

2001). While in our image, we didn't see any patches around, but a clear dust disk is shown. The major axis of the disk is about 658.8pc long.

Table 2.1: The Basic Properties of Radio Galaxies

Name(1)	R.A.(2)	Dec.(3)	Morphology(4)	logPt1.4(5)	logPc5(6)	logPj1.4(7)	Redshift(8)	Jet(9)	D(Mpc)(10)	m(11)	M(12)
3C 173.1	07 09 18.20	+74 49 32.0		26.41	24	23.86	0.292	N	1002.9	18.9	-21.251
B2 0915+32	09 18 58.00	+31 51 11.0		24	22.56	22.9	0.062	N	248	15.1	-21.933
NGC 3557	11 09 57.40	-37 32 17.0	E	22.8	21.42		0.0095	E	38.08	10.40	-22.885
NGC 3801	11 40 16.96	-17 43 39.5	S0	23.06	20.59		0.0105	SE	42	13.3	-19.937
NGC 3894	11 48 50.36	+59 24 56.4	S0	23.71	21.93	22.55	0.0109	SE	43.4	12.9	-20.404
NGC 4789	12 54 18.80	+27 04 13.4	E/S0	23.55	21.16		0.027	NW	108	13.3	-21.898
3C 278	12 54 37.30	-12 33 22.0		24.23	22.13		0.0138	E	55.2	13.5	-20.385
NGC 4839	12 57 24.31	+27 29 52.0		22.63	21.18	22.2	0.0249	N	99.6	13.69	-21.335
NGC 4869	12 59 23.38	+27 54 40.7	E	22.91	21.08	22.02	0.0235	NE	94	14.9	-20.003
NGC 4874	12 59 35.91	+27 57 30.8	S0	23.05	20.81		0.0232	NE	92.8	13.62	-21.251
NGC 5127	13 23 45.12	+31 33 56.6	E	23.85	21.77		0.0161	SE	64.4	13.9	-20.193
NGC 5141	13 24 51.67	+36 22 41.7	S0	23.42	22.38	22.45	0.0175	S	70	13.9	-20.369
IC 4296	13 36 38.80	-33 57 59.0	E	24.41	22.46	23.29	0.0129	NW	51.6	10.57	-23.208
NGC 5490	14 09 57.42	+17 32 43.4	E	23.68	22		0.0163	E	65.2	15.5	-18.661
3C 296	14 16 53.08	+10 48 25.2	S0	24.43	22.69		0.0237	SW	94.8	12.19	-22.776
B2 1422+26	14 24 40.52	+26 37 30.3	dG	24 22	.25	22.25	0.037	SE	148	15.62	-20.301
3C 305	14 49 21.37	+63 16 14.0	SB0	24.73	22.57		0.041	NE	164	13.74	-22.431
B2 1450+28	14 52 33.60	+27 57 54.0		24.56	22.56	23.81	0.1265	E	474.22		
PKS 1508+059	15 10 56.22	+05 44 41.6	E/S0	25.13	22.52		0.0767	NW	306.8	15.4	-22.074
4C 28.39	15 23 26.90	+28 37 32.0	dG	24.58	23.58	23.8	0.0825	SE	330	15.5	-22.19
B2 1613+27	16 15 31.41	+27 26 58.0		24.03	22.69	23.24	0.0647	S	258.8	14.9	-22.321
NGC 6166	16 28 38.30	+39 33 04.7	cG/dG	24.51	23.16		0.0303	E	121.2	12.61	-22.846
3C 352	17 10 44.05	+46 01 29.6		27.23	24.39	27	0.806	NW	2122.8	22.8	-18.943
B2 1827+32	18 28 56.70	+32 20 01.0		24.07	23.08	22.8	0.0659	E	263.6	15.1	-22.331
3C 388	18 44 02.37	+45 33 30.0		25.73	23.76	23.71	0.0908	SW	363.2	15.3	-22.765
3C 424	20 48 12.12	+07 01 17.5		25.67	23.6	24.34	0.127	NW	475.97	18.0	-20.705
NGC 7052	21 18 33.13	+26 26 48.7	E	22.72	22.1	21.66	0.0164	N	65.6	14.0	-20.486
PKS 2152-69	21 57 05.98	-69 41 23.7	S0	25.82	23.86		0.0282	NE	112.8	13.79	-21.472
NGC 7237	22 14 46.96	+13 50 25.9	S0	24.41	22.1		0.0268	NE	107.2	15	-20.366
3C 449	22 31 20.55	+39 21 29.6	E/S0	24.02	22.07	22.1	0.0171	N	68.4	13.15	-21.578
B2 2236+35	22 38 29.64	+35 19 45.1	E	23.44	21.83	22.83	0.0277	NE	110.8	15.0	-20.508
3C 452	22 45 48.77	+39 41 16.1	E	25.9	24.23	23.84	0.0811	SW	324.4	16.6	-21.409
UGC 367	00 37 05.39	+25 41 59.3	cG	23.13	21.77	22.3	0.0321	E	128.4	14.8	-20.876
3C 20	00 43 09.21	+52 03 33.5		26.52	23.07	24.42	0.174	NW	636.22	19	-21.368
NGC 326	00 58 22.70	+26 51 57.0	dG	24.61	22.29		0.0472	SE	188.8	13	-23.607
3C 29	00 57 37.98	-01 23 28.8	E	25.1	23.32		0.045	SE	180	14.07	-22.324
NGC 541	01 25 44.33	-01 22 46.6	E	23.53	21.79		0.0182	NE	72.8	13.61	-20.849
NGC 708	01 52 46.56	+36 09 06.6	E	22.62	21.31	21.93	0.016	W	64	14.8	-19.522
3C 68.2	02 34 23.89	+31 34 18.4		27.08	23.72		1.575	SE	2951.6	24	-18.816
3C 76.1	03 03 15.00	+16 26 20.0	E	24.52	21.94		0.0316	NW	126.4	14.86	-21.106
NGC 1316	03 22 41.50	-37 12 33.0	Sa	24.73	21.15	21.95	0.0063	SE	25.2	8.77	-23.306
NGC 1399	03 38 29.32	-35 27 00.7	ED	22.82	20.41	21.81	0.0049	S	19.6	9.90	-21.611
PKS 0405-12	04 07 48.43	-12 11 36.7		27.39	26.6		0.574	N	1699.5	14.86	-26.495
3C 270	12 19 23.25	+05 49 32.5	E	24.01	22.25		0.0073	E	29.2	10.4	-21.987
M 84	12 25 03.74	+12 53 13.1	E	23.24	21.72		0.0031	N	12.4	8.67	-21.931
NGC 315	00 57 48.88	+30 21 08.8	E	24.08	23.24		0.0167	SE	65.6	12.5	-21.8

Note: Col.(4):Morphology taken from NED. Col.(5):The total power at 1.4 GHz (W/Hz). Col.(6): The total power at 5 GHz (W/Hz). Col.(7): Jet power at 1.4 GHz (W/Hz). Col.(8): Redshift taken from NED. Col.(9): The direction of the radio jet. Col.(10): Distance derived from Hubble Law. Col.(11): Apparent Magnitude. Col(12): Absolute Magnitude in V band and corrected for galactic absorption.

Table 2.2: The Basic Properties of Normal Galaxies

Name	R.A.	Dec.	Morphology	Redshift	D(Mpc)	m	M
NGC 221	00 42 41.80	+40 51 54.6	dE	-0.000667	2.668	9.2	-18.136
NGC 547	01 26 00.62	-01 20 42.6	E	0.018239	72.956	13.34	-21.109
NGC 821	02 08 21.14	+10 59 41.7	E	0.005787	23.148	12.6	-19.587
NGC 1016	02 38 19.56	+02 07 09.3	E	0.021965	87.86	13.3	-21.521
NGC 1339	03 28 06.58	-32 17 10.0	E	0.004643	18.572	12.37	-19.018
NGC 1374	03 35 16.59	-35 13 34.5	S0	0.004316	17.264	12.30	-18.932
NGC 2325	07 02 40.53	-28 41 50.5	E	0.007702	30.808	13	-19.823
NGC 2300	07 32 20.49	+85 42 31.9	E	0.006464	25.856	12.2	-20.183
NGC 2434	07 34 51.16	-69 17 02.9	S0	0.004637	18.548	11.22	-20.942
NGC 2592	08 27 08.07	+25 58 13.2	E	0.006635	26.54	13.6	-18.72
NGC 2634	08 48 25.39	+73 58 01.8	E	0.007532	30.128	12.6	-19.867
NGC 2778	09 12 24.38	+35 01 38.9	E	0.006835	27.34	13.1	-19.153
NGC 2832	09 19 46.86	+33 44 59.2	E	0.023176	92.704	13.17	-21.721
NGC 2865	09 23 30.21	-23 09 41.2	E	0.008763	35.052	11.43	-21.567

Name	R.A.	Dec.	Morphology	Redshift	D(Mpc)	m	M
NGC 2872	09 25 42.53	+11 25 55.8	E	0.010811	43.244	13.0	-20.295
NGC 2986	09 44 16.04	-21 16 40.8	E	0.007679	30.716	10.93	-21.703
NGC 3078	09 58 24.59	-26 55 35.7	E	0.008322	33.288	11.07	-21.776
NGC 3348	10 47 10.00	+72 50 22.8	E	0.009463	37.852	12.0	-21.135
NGC 3377	10 47 42.40	+13 59 08.3	E	0.001908	7.632	10.7	-18.826
NGC 3605	11 16 46.61	+18 01 01.7	E/S0	0.002228	8.912	12.7	-17.119
NGC 3640	11 21 06.85	+03 14 05.4	E	0.004383	17.532	11.8	-19.58
NGC 3706	11 29 44.43	-36 23 28.7	E	0.00993	39.72	11.08	-22.238
NGC 3842	11 44 02.16	+19 56 59.3	E	0.021068	84.272	13.3	-21.399
NGC 3928	11 51 47.66	+48 40 59.3	S	0.003296	13.184	13.1	-17.565
NGC 4073	12 04 27.07	+01 53 45.5	E	0.019854	79.416	13.21	-21.365
NGC 4283	12 20 20.77	+29 18 39.2	E	0.003589	14.356	12.28	-18.588
NGC 4291	12 20 17.76	+75 22 15.2	E	0.005861	23.444	12.3	-19.671
NGC 4365	12 24 28.23	+07 19 03.1	E	0.004146	16.584	11.5	-19.668
NGC 4458	12 28 57.57	+13 14 30.8	E	0.002118	8.472	13.3	-16.419
NGC 4473	12 29 48.87	+13 25 45.7	E	0.007485	29.94	11.2	-21.275
NGC 4478	12 30 17.42	+12 19 42.8	E	0.0045	18	12.2	-19.158
NGC 4551	12 35 37.97	+12 15 50.4	E	0.003909	15.636	13.1	-17.999
NGC 4564	12 36 26.99	+11 26 21.5	E	0.003809	15.236	12.2	-18.83
NGC 4621	12 42 02.32	+11 38 48.9	E	0.001368	5.472	11.0	-17.801
NGC 4648	12 41 44.39	+74 25 15.4	E	0.004917	19.668	12.6	-18.937
NGC 4673	12 45 34.69	+27 03 38.8	S0	0.022856	91.424	13.7	-21.153
NGC 4709	12 50 04.02	-41 22 56.9	S	0.015604	62.416	13.42	-20.949
NGC 4786	12 54 32.42	-06 51 33.9	E	0.015501	62.004	14	-20.081
NGC 4782	12 54 35.72	-12 34 07.1	E	0.013279	53.116	13	-20.8
NGC 4889	13 00 07.68	+27 58 32.8	E	0.021321	85.284	13.05	-21.636
NGC 4936	13 04 17.10	-30 31 34.6	E	0.010397	41.588	11.32	-22.049
NGC 4952	13 04 58.38	+29 07 20.3	E	0.019907	79.628	13.01	-21.536
NGC 5017	13 12 54.50	-16 45 57.0	E	0.008483	33.932	14	-18.931
NGC 5044	13 15 23.97	-16 23 07.9	E	0.021348	85.392	12	-22.892
NGC 5061	13 18 05.07	-26 50 14.0	E	0.008876	35.504	10.41	-22.569
NGC 5173	13 28 25.30	+46 35 29.6	E	0.008069	32.276	13.5	-19.139
NGC 5198	13 30 11.40	+46 40 14.8	E	0.008449	33.796	13.2	-19.521
NGC 5322	13 49 15.20	+60 11 25.5	E	0.005941	23.764	11.3	-20.627
NGC 5557	14 18 25.71	+36 29 37.0	E	0.010717	42.868	12.2	-20.98
NGC 5576	14 21 03.68	+03 16 15.6	E	0.004943	19.772	12.3	-19.284
NGC 5812	15 00 55.70	-07 27 26.5	E	0.006438	25.752	12	-20.342
NGC 5845	15 06 00.78	+01 38 01.7	E	0.004857	19.428	13.8	-17.819
NGC 6495	17 54 50.76	+18 19 36.9	E	0.010431	41.724	13.8	-19.555
NGC 6849	20 06 15.62	-40 11 53.9	E	0.020147	80.588	13.5	-21.273
NGC 6876	20 18 19.15	-70 51 31.7	S0	0.013646	54.584	11.54	-22.34
NGC 7014	21 07 52.17	-47 10 44.4	E/S0	0.016201	64.804	12.25	-21.933
NGC 7562	23 15 57.50	+06 41 15.1	E	0.012035	48.14	13	-20.761
NGC 7619	23 20 14.52	+08 12 22.5	E	0.012549	50.196	12.7	-20.064

Table 3.1: Dust Properties of Radio Galaxies

Name	Dust?	Dust Morphology	Size	Name	Dust?	Dust Morphology	Size
3C 173.1	X			B2 1827+32	X		
B2 0915+32	✓	dust patches	1847.3pc	3C 388	X		
NGC 3557	✓	face-on dust disk	729pc	3C 424	X		
NGC 3801	✓	abundant dust	6256.6pc	NGC 7052	✓	edge-on dust disk	1954.4pc
NGC 3894	✓	dust patches, filaments	1475.2pc	PKS 2152-69	✓	dust patches, filaments	1800pc
NGC 4789	✓	dust disk	459.6pc	NGC 7237	X		
3C 278	X			3C 449	✓	dust torus	1819.5pc
NGC 4839	X			B2 2236+35	X		
NGC 4869	X			3C 452	X		
NGC 4874	X			UGC 367	✓	dust ring	1639.2pc
NGC 5127	✓	dust torus	1507.6pc	3C 20	X		
NGC 5141	✓	dust disk	1117.3pc	NGC 326	X		
IC 4296	✓	dust disk	658.8pc	3C 29	X		
NGC 5490	X			NGC 541	✓	face-on dust ring	1161pc
3C 296	✓	dust disk	807pc	NGC 708	✓	dust lanes, patches	3745.5pc
B2 1422+26	X			3C 68.2	X		
3C 305	✓	dust lanes, patches	13087.5pc	3C 76.1	✓	dust disk	1345pc
B2 1450+28	X			NGC 1316	✓	clumpy dust, filaments	2010pc
PKS 1508+059	X			NGC 1399	X		
4C 28.39	X			PKS 0405-12	X		
B2 1613+27	X			3C 270	✓	dust disk	373.2pc
NGC 6166	✓	dust filaments	1934.5pc	M 84	✓	dust lanes, patches	1056pc
3C 352	X			NGC 315	✓	dust disk, lanes	1326.2pc

The estimated sizes of dust disks are their lengths of the diameters, and the estimated sizes of dust lanes or filaments are their extended lengths

3.2 NGC 315

NGC 315 is a member of Zwicky cluster 0107.5+3212 (Zwicky et al. 1961), which is located in the Perseus-Pisces filament. This galaxy presents a radio jet in position P.A.310º with a possible counter jet (Bridle et al. 1979). Butcher, van Breugel, and Miley (1980) did not find any optical counterpart of the radio jet from their blue image. Colina, L. (1990) showed that this elliptical galaxy with its major optical axis is in a direction perpendicular to the observed radio jet. Verdoes Kleijn, G.A. et al. (1999) detected a central dust disk 820 pc in diameter that is close to but not perfectly an ellipse; the northern tip of the disk has a small extension. In addition, several mottled patches of dust are detected southwest of the nucleus out to 1.5kpc. The central part of the dust disk forms a small, bright emission-gas disk, which extends into low-level emission throughout the dust disk. There is also a low-level emission feature adjacent to the southeast side of the dust disk that is elongated in the direction of the dust disk. See also Capetti, A. et al. (2000). While in our residual image, we estimate the diameter to be about 1326.2pc, larger than the value Verdoes Kleijn, G.A. et al. gave in 1999.

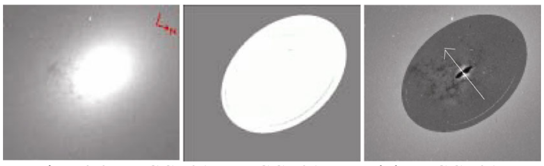

Fig. 3.2: NGC 315, NGC 315 model, NGC 315 subtracted

3.3 PKS 2152-69

Many dark features appeared after galaxy model is subtracted. No relevant articles were published on this object before. The irregular dust structures extend to about 3,480pc in the direction of southeast.

Fig. 3.3: PKS 2152-69, PKS 2152-69 model, PKS 2152-69 subtracted

3.4 NGC 1316

NGC 1316 is an extended source, and it has a compact core. It locates in the Fornax cluster. It also has close or interacting companion. The very irregular and prominent dust patterns makes this one of the most outstanding radio galaxies (Wade, 1960b). A kinematics study by Searle (1965) suggested that the dust is in a plane seen nearly "face-on", possibly explaining the irregular appearance. In our residual image, we could see the marvelous dust structures in much detail. The distribution is not uniform and a symmetrical. These extend to about 1,474pc.

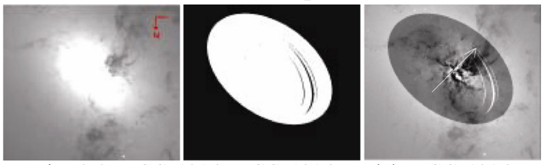

Fig. 3.4: NGC 1316, NGC 1316 model, NGC 1316 subtracted

3.5 NGC 4551

NGC 4551 is a member of the Virgo cluster and has an uncertain classification as elliptical . It is in a non-interacting pair with NGC 4550 at 3 arcmin. The structures of the dust lanes are marvelous, which extend about 1,693.2pc.

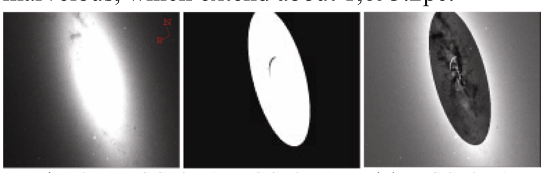

Fig. 3.5: NGC 4551, NGC 4551 model, NGC 4551 subtractecd

3.6 NGC 4936

The filaments are distinctly seen in our residual image. They stretch about 1,993.5pc in length.

Fig. 3.6: NGC 4936, NGC 4936 model, NGC 4936 subtracted

3.7 NGC 5173

The vortex morphology of dust showed up after galaxy model subtraction. They extend about 1,372pc.

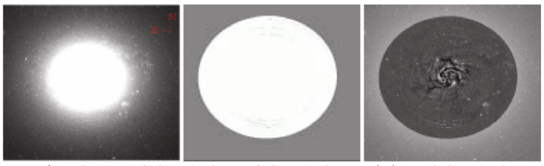

Fig. 3.7: NGC 5173, NGC 5173 model, NGC 5173 subtracted

4. Discussion

4.1 The Detection of Dust

Dust is detected in 22 out of 46 radio galaxies, and is also detected in 14 out of 58 normal galaxies. We address the confidence level that the detection rates can give in our limited sample. We calculate the probability distribution of each sample. First we assume the total sample N→∞ in the real world. Among N, the ratio of a galaxy with dust is ρ, while on the other hand, the ratio of no dust is 1-ρ. From Bayes' theorem, the probability distribution of ρ from our observed samples is:

Probability $\propto C_{22}^{46}\rho^{22}(1-\rho)^{24}\,d\rho$

The normalization

$$C_{22}^{46} A\int_0^1 \rho^{22}(1-\rho)^{24}\,d\rho = \int_0^1 f(\rho) = 1$$

According to the Beta Function:

$$B(z,w) = B(w,z) = \int_0^1 t^{z-1}(1-t)^{w-1}dt \quad (4.1)$$

which is related to the Gamma Function:

$$B(z,w) = \frac{\Gamma(z)\Gamma(w)}{\Gamma(z+w)} \quad (4.2)$$

we get A=47, so the probability is

$$f(\rho) = \frac{\rho^{22}(1-\rho)^{24}}{B(23,25)} \quad (4.3)$$

The mean probability is

$$\mu_\rho = \int_0^1 \rho f(\rho)d\rho \quad (4.4)$$

$$\mu_\rho = \int_0^1 \rho f(\rho)d\rho$$

$$= \frac{B(24,25)}{B(23,25)} = 0.479 \quad (4.5)$$

The standard deviation

$$\sigma_\rho^2 = \int_0^1 (\rho - \mu_\rho)^2 f(\rho)d\rho \quad (4.6)$$

$$= \frac{1}{B(23,25)}[B(25,25) - 2\times\mu_\rho\times B(24,25)$$

$$+\mu_\rho^2\times B(23,25)]$$

$$=0.00509 \quad (4.7)$$

$$\sigma = 0.07134 \approx 7.13\% \quad (4.8)$$

We also use the same method to estimate the mean probability and the standard deviation of detection rates in the normal galaxy samples. The dust detection rate is (48 ± 7.1%) for radio galaxies and (25 ± 5.5%) for normal galaxies, which implies that the ratio difference is significant.

4.2 The Correlations Between Dust and General Properties of Galaxies

We further study on the distribution and relations among the properties, such as redshift, absolute magnitude, core radio power, and total radio power, of our sample.

The K-S test (Press et al. 1992) was applied to verify if these properties are from same parent distributions between dust and dust-free radio galaxies. The probability that the sample distributions of absolute magnitude, redshift, total power, and core power are drawn from the same parent population is 76.1%, 0.08%, 4.6%, and 16.5%, respectively. When we compare different distributions or compute correlation coefficients, we consider as “statistically significant” these differences or correlations with a probability to appear by chance being less than 10%. In the case of the distributions of redshift and total power, the K-S test gives a probability of 0.08% and 4.6%. We could probably conclude that the distributions of redshift is quite different between the two samples: radio galaxies with dust and without. This indicates that we could find more distributions of dust in nearby radio galaxies than distant ones. It may simply be due to the detection limit of our detectors. If not, this result implies that nearby radio galaxies contain more dust than the distant ones. If the origins of these dust are internal, that is, they form and evolve together with the galaxies, then at their early stage, they may still spread in the entire space and have no sufficient time to settle down into an equilibrium state. Their diffuse appearance might be too sparse for us to detect using our analytic methods. While in appearances of dust disks or filaments, they are probably easier to be seen. In the case of

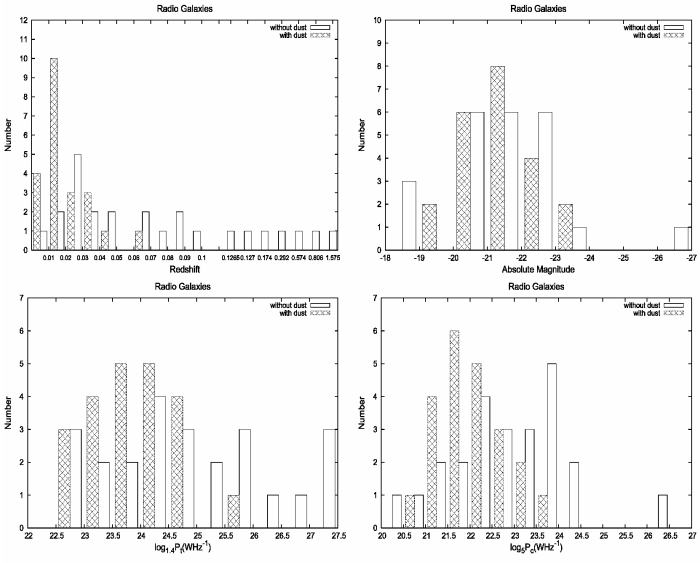

Fig. 4.1: Distribution of the redshift, absolute magnitude, total radio power, and the core radio power for the radio galaxies. (dashed and open histograms representing with and without dust, respectively)

total power, there might exist difference of the distributions of dust between radio galaxies with different total power. In this figure, we see radio galaxies with less power having a tendency to contain dust than radio galaxies with more power. This indicates that the formation of nuclear dust and the total power of the whole galaxy are correlated. Probably there is an mechanism which generates radio emission but also facilitates the formation and evolution of dust. We have to make further studies to examine the origins of dust and to know the emission mechanism in radio. In the distributions of absolute magnitude and core power, radio galaxies with dust match those of the radio galaxies without. So, the optical absolute magnitude and core power are not the critical factors influencing the existence of dust near the galaxy nuclei.

K-S test is also applied to examine the distributions for normal galaxies plotted above. The probabilities that the sample distributions of redshift and absolute magnitude are drawn from the same parent population : 78.3% and 33.8%. These suggest that there exists no difference in redshift and absolute magnitude between normal galaxies with dust and without

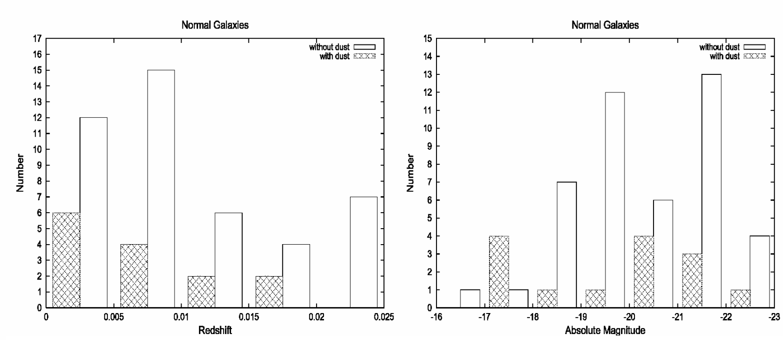

Fig. 4.2: Distribution of the redshift and absolute magnitude for the normal galaixes.(dashed and open histograms representing with and without dust, respectively)

4.3 The Orientation of Radio Jets and Dust Disks

We could see several different dust morphologies in our residual images presented in Chapter 4. Some are disk-like, some are lanes and torus, and others are filamentary. It is interesting to investigate the correlation between dust morphology and radio source using higher resolution data which provide information closer to the nucleus where the interaction is likely to be more important. Interestingly, we find that the directions of radio jets are nearly perpendicular to the planes of dust disks. The approximate angles between the radio jets and the normal direction of the plane we measured are listed in Table 4.1.

Table 4.1: Radio galaxies with dust disk

Name	angle	Size	
NGC 7052	0.	1954.4	pc
UGC 367	0.	1639.2	pc
NGC 315	0.	1326.2	pc
3C 76.1	10.	1345	pc
NGC 5141	10.	1117.3	pc
3C 270	10.	373.2	pc
3C 296	15.	807	pc
NGC 5127	20.	1507.6	pc
IC 4296	22.	658.8	pc
NGC 4789	25.	459.6	pc

We can roughly conclude that, if the dust disks are clearly seen, the angles between the radio jets and the normal directions of disk planes are small. De Koff et al. (2000) found that for FRI sources with dust disks of size less than 2.5kpc, the radio jet lies within 15° of the disk axis. According to the widely accepted AGN model, jets are ejected from the central accretion disk, and perpendicular to the disk. The estimated size of accretion disk is about several AU, rather smaller than the size of dust disk (several hundred of pc). If the evidences from future observations show that the radio jets are indeed nearly perpendicular to the planes of dust disks, we may infer that the inner planes of accretion disk and the outer dust disk planes are co-align. It has great scientific significance. We may be able to find the theoritical accretion disk by tracing the direction of the dust disk. Dust disks may play the role of providing the fuel to the central nuclei. We ask us the following questions: Is the existence of dust disks important to the existence of central black holes? Are they correlated?

4.4 Estimation of Dust Mass

In this thesis, we follow Sadler & Gerhard (1985)and van Dokkum & Franx (1995) to estimate the dust mass present in the nuclei of our galaxies. The dust mass is given by

$$M = \langle A_v \rangle \sum \Gamma^{-1} \quad (4.9)$$

where $\langle A_v \rangle$ is the mean visual extinction in

Table 4.2: Estimation of dust mass for radio galaxies

Name	Int_{model}	Mean Int_{res}	σ_{res}.	pixels Σ_{res}.	Int_{obs}	τ	A_v	Mass	LogM
B2 0915+32	489024	-0.086	0.854	682	484971	0.008	0.012	1.366×10^6	6.135
NGC 3557	41606400	0.519	3.069	1244	41558560	0.001	0.001	3.444×10^5	5.537
NGC 3801	2715520	0.059	1.465	8325	2660015	0.020	0.029	4.138×10^7	7.617
NGC 3894	5273600	0.053	1.547	3446	5243369	0.005	0.008	4.768×10^6	6.678
NGC 4789	3700480	0.213	1.431	229	3698393	0.001	0.001	3.108×10^4	4.492
NGC 5127	1673600	-0.043	1.591	687	1665498	0.005	0.007	8.023×10^5	5.904
NGC 5141	1645440	-0.046	1.511	534	1637780	0.004	0.006	5.996×10^5	5.778
IC 4296	22566400	0.387	3.412	592	22521926	0.002	0.002	2.811×10^5	5.449
3C 296	3733760	-0.079	1.680	188	3730717	0.001	0.001	3.688×10^4	4.567
3C 305	956800	1.388	1.662	3981	928999	0.029	0.042	2.825×10^7	7.451
NGC 6166	850560	-0.083	1.564	291	848100	0.0028	0.004	2.028×10^5	5.307
NGC 7052	1086720	0.054	1.823	767	1077904	0.008	0.011	1.503×10^6	6.177
PKS 2152-69	1592320	0.090	1.273	2150	1572958	0.012	0.017	6.329×10^6	6.801
3C 449	2398080	-0.212	2.047	684	2389632	0.003	0.005	5.809×10^5	5.764
UGC 367	624512	-0.168	0.956	487	621384	0.005	0.007	5.883×10^5	5.77
NGC 541	1601280	0.105	1.579	305	1599211	0.001	0.001	9.487×10^4	4.977
NGC 708	27680000	-1.332	4.849	6252	27379212	0.011	0.015	1.644×10^7	7.216
3C 76.1	302528	0.031	1.302	119	301144	0.004	0.006	1.312×10^5	5.118
NGC 1316	50547200	-0.304	11.750	17987	48317528	0.045	0.065	1.952×10^8	8.29
3C 270	9587200	-1.206	2.551	383	9577714	0.001	0.001	9.124×10^4	4.96
M 84	20320000	0.555	2.667	7231	20172250	0.007	0.011	1.269×10^7	7.103
NGC 315	2698240	-0.411	2.155	1029	2679777	0.007	0.009	1.700×10^6	6.23

Table 4.3: Estimation of dust mass for normal galaixes

Name	Int_{model}	Mean Int_{res}	σ_{res}.	pixels Σ_{res}.	Int_{obs}	τ	A_v	Mass	LogM
NGC 2434	9171200	-0.130	4.102	403	9153444	0.002	0.003	1.879×10^5	5.274
NGC 2865	33286400	-2.372	6.839	355	33256929	0.001	0.001	7.568×10^4	4.879
NGC 2872	6136960	0.134	1.769	240	6131872	0.001	0.001	4.790×10^4	4.68
NGC 3078	10316800	-1.558	2.402	380	10297904	0.002	0.003	1.667×10^5	5.225
NGC 3605	1813760	0.148	1.467	4257	1771722	0.023	0.034	2.402×10^7	7.381
NGC 3928	2240000	0.729	1.281	10847	2147746	0.042	0.060729376	1.098×10^8	8.041
NGC 4283	9324800	-0.212	2.560	3873	9275701	0.005	0.008	4.291×10^6	6.692
NGC 4551	6656000	2.157	4.186	4350	6571383	0.013	0.018	1.339×10^7	7.127
NGC 4786	4819200	-0.057	2.592	383	4809561	0.002	0.003	1.845×10^5	5.266
NGC 4936	16665600	1.174	5.147	4926	16520217	0.009	0.012	1.039×10^7	7.017
NGC 4952	2397440	-0.062	1.663	249	2394411	0.001	0.002	7.576×10^4	4.879
NGC 5173	3777280	0.133	1.480	2740	3754466	0.006	0.008	3.995×10^6	6.602
NGC 5322	14649600	-0.829	3.828	525	14540410	0.007	0.011	9.452×10^5	5.976
NGC 5845	6049280	-0.715	1.791	174	6034498	0.002	0.004	1.024×10^5	5.01

magnitudes, Σ is the surface area covered by dust, and Γ is the extinction coefficient per unit mass. We adopt $\Gamma = 6\times10^{-6}$ mag kpc^2 $M_\odot^{-1}$ (van Dokkum & Franx 1995).

To obtain $\langle A_v \rangle$, we have to determine the optical depth. The optical depth in R is $\tau = -\ln(F_{obs}/F_{mod})$, where F_{obs} is the observed flux and F_{mod} is the modeled flux, and $A_R = 1.0857\tau$. Assuming a Galactic extinction law with R_v=3.1, we have A_v=1.33A_R (Cardelli, Clayton, & Mathis 1989). We thus sum the pixels whose values are less than 3σ of the residual images. The details are listed as above tables.

The average value of log$M$ in radio galaxies is 6.0600 and its σ is 1.0041. While in normal galaxies, the average value of log$M$ is 6.0035 and its σ is 1.0731.

We also compare the dust mass with the properties such as redshift, absolute magnitude, total power, and core power in each radio galaxies and normal galaxies.

Next we turn to testing the correlations between each properties of radio galaxies, in which most useful is the linear correlation coefficient. For pairs of quantities (x_i, y_i), i=1,...,N, the linear correlation coefficient r is given by the formula

$$r = \frac{\sum_i (x_i - \bar{x})(y_i - \bar{y})}{\sqrt{\sum_i (x_i - \bar{x})^2}\sqrt{\sum_i (y_i - \bar{y})^2}} \qquad (4.10)$$

where, as usual, $\bar{x}$ is the mean of the x_i's, $\bar{y}$ is the mearn of the y_i's.

The value of r lies between -1 and 1, inclusive. It takes on a value of 1, termed "complete positive correlation," when the data points lie on a perfect straight line with positive slope, with *x* and *y* increasing together. If the data points lie on a perfect straight line with negative slope, *y* decreasing as *x* increases, then *r* has the value -1; this is called "complete negative correlation." A value of *r* near zero indicates that the variables *x* and *y* are *uncorrelated*.

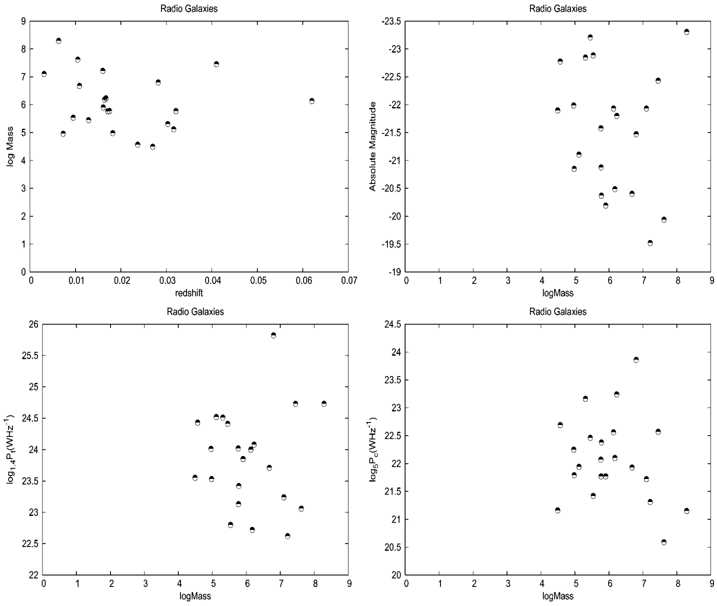

Fig. 4.3:Distribution of the redshift, absolute magnitude, total radio power, and the core radio power versus dust mass in unit of solar mass for radio galaxies.

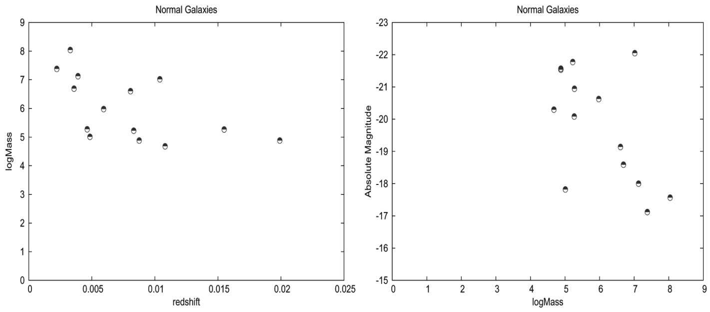

Fig. 4.4:Distribution of the redshift and absolute magnitude versus dust mass for normal galaxies.

The probability density that any random sample of uncorrelated experimental data points would yield an experimental linear-correlation coefficient equal to r is given by

$$p(r;v) = \frac{1}{\sqrt{\pi}} \frac{\Gamma[(v+1)/2]}{\Gamma(v/2)} \left(1 - r^2\right)^{(v-2)/2} \qquad (4.11)$$

where v =N-2 is the number of degrees of freedom for an experimental sample of N data points (Philip, R.B. and D.Keith Robinson 2002).

The probability $p(r;v)$ that a random sample of *N* uncorrelated data points would yield an experimental linear-correlation coefficient as large as or large than the observed value of |r|. This probability is the integral of $p(r;v)$ for v =N-2:

$$p(r;v) = 2\int_{|r|}^{1} p_x(r;v)dr \qquad (4.12)$$

A small value of $p(r;v)$ implies that the observed variables are probably correlated.

According to Equation (4.11) and (4.12), we compute the linear correlation coefficient and the probability of each figure. The results are displayed here:

In radio galaxies, these results give us a large possibility that the dust mass are correlated to neither redshift, total power, nor core power. In normal galaxies, redshift and absolute magnitude might both relate to the dust mass. If this is really the case, it means that, the absolute magnitude will gradually decrease with more nuclear dust. This is easy to understand. If a galaxy contains more dust, dust would absorb or shield the light from the nucleus. The galaxy would look dimmer than the other ones. Redshift and logMass in normal galaxies are nearly anti-correlated. It might simply be due to selection effect from the detection limit of the detectors. If the origin of the dust is internal, that is, dust grows and evolves with the whole galaxy, then it requires time to settle down from the distributions of diffuse state to lanes or even disks. Our estimation of dust mass is more suitable for the form of disks, and lanes which are clearly seen, rather than for the filamentary ones. We need more sensitive equipments to detect the existence of nuclear dust and more accurate dust mass estimation methods to do further confirmation.

5. Summary and FutureWork

(1) In our samples of radio galaxies and normal galaxies, we conclude that the dust detection rate is about 48% in radio galaxies, and about 24% in normal galaxies.

(2) Some sources have not been detected with nuclear dust before, such as NGC 4789, PKS 2152-69, NGC 2434, NGC 2872, NGC 3078, NGC 4786, NGC 4952, NGC 5845, NGC 4283, NGC 4551, NGC 4936, and NGC 5173. In their detailed residual images, the dust in most of them are clearly seen.

(3) We compare the essential properties between galaxies with dust and without.

(4) We discuss the orientations of radio jets and the dust disks. For some galaxies, the orientations are aligned; while in others, there are still some small angles between the radio jets and the normal directions of disk planes.

(5) We use the absorption method to estimate the mass of dust. The results are also presented and compared with their essential properties.

(6) Usually galaxies with high redshift have high radio power. So we should confine one critical factor and then compare the other factor to see if this is really the case that affects the existence of dust.

(7) A systematic and more detailed observation in multi-wavelengths and even spectroscopic observation is needed.

(8) The question is raised that why the normal elliptical galaxies that also show similar dust distributions near their cores do not host AGNs. Are these normal galaxies lacking a massive black hole to accrete the material and to convert the gravitational energy? Or is the fuel, such as the dust disk, not funneled effectively to the nucleus? What are their operations of mechanisms?

(9) An elliptical galaxy can undergo merging with a dust rich galaxy, or it can acquire dust by tidal stripping with a nearby galaxy. After the interaction, the dust is expected to be distri- buted throughout the galaxy in a filamentary distribution. It will begin to settle into an equilibrium state and regular orbit around the nucleus. The formation of gaseous disks takes place after a few orbits

around the accreting galaxy, i.e., in about 0.5-2 Gyr after capture (Steinman-Cameron 1991). This implies that the origin of the dust is closely related to the evolutionary history of the parent galaxy. We will thus examine the dynamical state of the dust to further understand the phenomenon.

Reference

Bridle, A.H., Davies, M.M., Fomalont, E.B., Willis, A.G., and Strom, R.G., 1979, *ApJL*, 228, 9

Butcher, H.R., van Breugel, W., and Miley, G.K., 1980, *ApJ.*, 235, 749

Capetti, A., & Celotti, A., 1999, *MNRAS*, 304, 434

Capetti, A., de Ruiter, H.R., Fanti, R., et al., 2000, *A&A*, 362, 871

Colbert, J.W., Mulchaey, J.S., Zabludoff, A.I., 2001, *AJ*, 121, 808

Colina, L., 1990, *AJS*, 72, 41

de Juan, L., Colina, L., & Golombek, D., 1996, *A&A*, 305, 776

de Koff, S., Baum, S.A., Sparks, W.B., et al., 1996, *ApJS*, 107, 621

de Koff, S., Best, P., Baum, S.A., Sparks, W., Rottgering, H., Miley, G., Golombek, D., Macchetto, F., Martel, A., 2000, *ApJS*, 129, 33

de Ruiter, H.R., Parma, P., Capetti, A., Fanti, R., Morganti, R., 2002, *A&A*, 396, 857

Ebneter, K., Balick, B., 1985, *AJ*, 90, 2

Ferrari, F., Pastoriza, M.G., Macchetto, F., & Caon, N., 1999, *A&AS*, 136, 269

Gonzalez-Serrano, J.I. et al., 1989, *AJL*, 338, 29

Goudfrooij, P., Hansen, L., Jorgensen, H.E., &Norgaard-Nielsen, H.V., 1997, *A&AS*, 105, 341

Jaffe, W., Ford, H.C., Ferrarese, L., van den Bosch, F., & O'Connell, R.W., 1993, *Nature*, 364, 213

Jedrzejewski, R.I., 1987, *MNRAS*, 226, 747

Jester, S., 2003, *NewAR*, 47, 427

Kotanyi, C.G., and Ekers, R.D., 1979, *Astr.Ap.*, 73, L1

Liu, F.K., and Zhang, Y.H., 2002, *A&A*, 381, 757

Martel, A.R., Baum, S.A., Sparks, W.B., et al., 1999, *ApJS*, 122, 81

Press, W.H., Tenkolsky, S.A., Vetterling, W.T., & Flannery, B.P., 1992, *Numerical Recipes*, Cambridge Univ. Press, Cambridge

Sadler, E.M., & Gerhard, O.E., 1985, *MNRAS*, 214, 177

Searle, L., 1965, *Nature*, 207, 1282

Sparks, W.B., Baum, S.A., Biretta, J., Macchetto, F.D., 2000, *AJ*, 542, 667

Tomita, A., Aoki, K., Watanabe, M., Takata, T., & Ichikawa, S., 2000, *AJ*, 120, 123

Tran, H.D., Tsvetanov, Z., Ford, H.C., Davies, J., 2001, *AJ*, 121, 2928

van Dokkum, P.G., and Franx, M., 1995, *AJ*, 110, 5

Verdoes Kleijn, G.A., Baum, S.A., de Zeeuw, P.T., & O'Dea, C.P., 1999, *AJ*, 118, 2592

V'eron-Cetty, M.-P. & V'eron, P., 1988, *A&A*, 204, 28

Wade, C.M. 1960b, *Pub.N.R.A.O*, 1, 6